AIAA JOURNAL
Vol. 34, No. 11, November 1996

Nonlinear Dynamic Buckling of a Cylindrical Shell Panel Model

Anthony N. Kounadis* and Dimitris S. Sophianopoulos†
National Technical University of Athens, Athens 10682, Greece

The dynamic buckling response of a spring-mass, geometrically imperfect, dissipative model with 3 degrees of freedom simulating a relatively deep cylindrical shell panel under step loading is comprehensively analyzed. The main feature of the real continuous structure and its corresponding model is that, under the same loading statically applied, both exhibit snapping. Energy, topological, and geometric considerations allow us to establish qualitative and quantitative criteria leading to dynamic buckling loads of both dissipative and nondissipative models without integrating the highly nonlinear equations of motion. An a priori knowledge of the accuracy of these buckling estimates is successfully obtained by discussing the geometry of the channel in which the motion takes place before reaching the escape passage through a saddle (or its neighborhood) with very small negative total potential energy. A comparison of the numerical results obtained by the proposed method with those of Runge–Kutta–Verner scheme shows the reliability and efficiency of the proposed method.

I. Introduction

QUITE often in engineering practice the dynamic behavior of (actual) continuous structures is simulated by that of simple models with a few degrees of freedom (DOF). This is achieved by using various matching criteria with the aid of which the response of the actual structure can be successfully approximated, quantitatively and qualitatively, through the dynamic analysis of its corresponding model.

In this analysis, a relatively deep shell panel under a step point-loading of infinite duration transversely applied,[1] is assumed to be simulated by a one-mass undamped spring-model with 3 DOF (Fig. 1), presented by Greer and Palazotto.[2] The shell panel under normal loading exhibits a limit-point (snapping) instability.[3,4] This is the main feature that must be taken into account in seeking the equivalent shell model; it was used by Greer and Palazotto[2] as a tool for finding suitable integration time steps for nonlinear finite element analysis. Because the dynamic buckling analysis of any real structure must include small initial imperfections as well as geometric nonlinearities and damping, all of these parameters are taken into account in the subsequent analysis.

The geometrically imperfect cylindrical shell model shown in Fig. 2 under a statically applied load exhibits a limit-point instability, and hence the readily applied dynamic buckling analysis developed by Kounadis[5] can be employed successfully.

A. Description of the Model

All four translational springs of the model shown in Fig. 2 having the same length l are linearly elastic with stiffnesses k_i ($i = 1, 2, 3, 4$). Springs 1 and 2 remain horizontal throughout deformation, with their ends sliding freely on vertical tracks. Springs 3 and 4 are free to rotate in any direction on their simply supported ends. Hence, only geometric nonlinearities are taken into account. Because no rotational springs are present, no bending action is included and thus only membrane action is considered. The effect of longitudinal stiffness (u direction) on the transverse deflection w is neglected because of the panel's greater length compared to the other dimensions. Moreover, the interactions of motions at various points of the shell panel are disregarded.

The limits and reliability of the (perfect nondissipative) model to represent an actual shell panel have been discussed in previous studies.[2,6] The initial unstressed configuration is defined by the displacement components u_o, v_o, and w_o of the mass m of the model in the directions x, y, and z (attributable to unavoidable imperfections), while the deformed (stressed) configuration in the phase space is defined by the displacement components u, v, and w, and their corresponding velocities $\dot{u}$, $\dot{v}$, and $\dot{w}$, where the dot denotes differentiation with respect to time t. The model is subjected to a step-point loading of infinite duration, $P(t) = P$, applied vertically at the center of the mass.

In view of the above, it is clear that the stiffness of the model is provided mainly by springs 3 and 4, and the presence of springs 1 and 2 is of secondary importance.

B. Geometric Considerations

Let us first consider the geometrically perfect model shown in Fig. 1, where the mass of the model is located at the origin O. Under the action of the point load, the new position of the origin O' is defined by the displacement components u, v, and w. The new lengths of the stressed springs ($i = 1, 2, 3, 4$) are given by

$$l_1' = [v^2 + (l-u)^2]^{\frac{1}{2}}, \qquad l_2' = [v^2 + (l+u)^2]^{\frac{1}{2}}$$
$$l_3' = [(h-w)^2 + (d+v)^2 + u^2]^{\frac{1}{2}} \tag{1}$$
$$l_4' = [(h-w)^2 + (d-v)^2 + u^2]^{\frac{1}{2}}$$

where h and d distances are invariable with time, such that $h^2 + d^2 = l^2$.

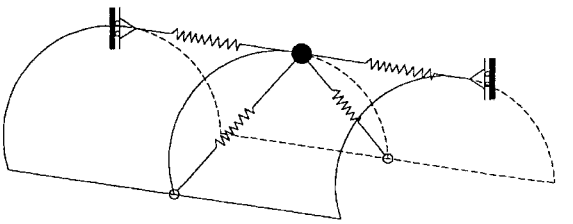

a) Panel

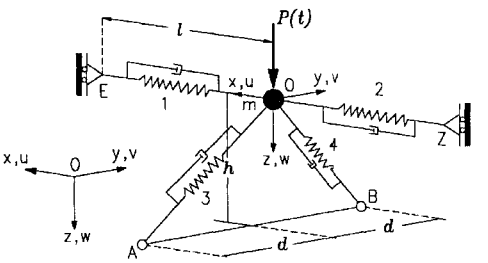

b) Panel's one-mass 3-DOF spring dissipative model

Fig. 1 Cylindrical shell.

Received Nov. 17, 1995; revision received May 20, 1996; accepted for publication June 8, 1996.

*Professor, Department of Civil Engineering, Structural Analysis and Steel Bridges.

†Research Engineer, Department of Civil Engineering, Structural Analysis and Steel Bridges.

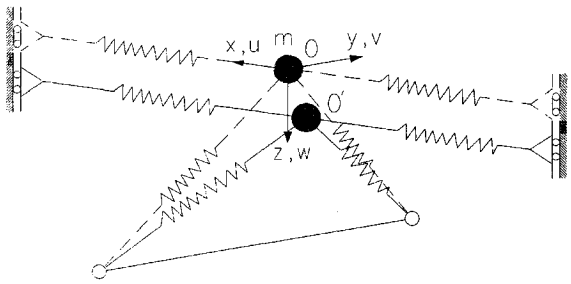

Fig. 2 Geometrically imperfect one-mass spring model with 3 DOF.

The lengths of the unstressed springs of the initial geometrically imperfect model l_{i0} ($i = 1, 2, 3, 4$), shown in Fig. 2, attributable to Eq. (1), are equal to

$$l_{10} = \left[v_0^2 + (l - u_o)^2\right]^{\frac{1}{2}}, \qquad l_{20} = \left[v_0^2 + (l + u_o)^2\right]^{\frac{1}{2}}$$
$$l_{30} = \left[(h - w_o)^2 + (d + v_o)^2 + u_o^2\right]^{\frac{1}{2}} \tag{2}$$
$$l_{40} = \left[(h - w_o)^2 + (d - v_o)^2 + u_o^2\right]^{\frac{1}{2}}$$

In view of Eqs. (1) and (2), the translational displacements δ_i ($i = 1, 2, 3, 4$) of the four springs are given by

$$\delta_1 = l_1' - l_{10} = [v^2 + (l - u)^2]^{\frac{1}{2}} - \left[v_o^2 + (l - u_o)^2\right]^{\frac{1}{2}}$$

$$\delta_2 = l_2' - l_{20} = [v^2 + (l + u)^2]^{\frac{1}{2}} - \left[v_o^2 + (l + u_o)^2\right]^{\frac{1}{2}}$$

$$\delta_3 = l_3' - l_{30} = [(h - w)^2 + (d + v)^2 + u^2] - \left[(h - w_o)^2 + (d + v_o)^2 + u_o^2\right]^{\frac{1}{2}} \tag{3}$$

$$\delta_4 = l_4' - l_{40} = [(h - w)^2 + (d - v)^2 + u^2]^{\frac{1}{2}} - \left[(h - w_o)^2 + (d - v_o)^2 + u_o^2\right]^{\frac{1}{2}}$$

II. Mathematical Analysis

The response of the spring model under static loading P can be described properly via the total potential energy function $V = V(u, v, w; u_o; v_o; w_o; P)$. We postulate that V is a well-behaved single-valued function having partial derivatives with respect to u, v, w and P, which always exist and are always continuous, at least in the domain of interest. For a fixed value of P, the total potential energy V represents a hypersurface in the four-dimensional configuration space spanned by V and u, v, w. We can imagine a series of energy hypersurfaces corresponding to different but constant values of P. As is known, equilibrium paths (in the four-dimensional load-displacement space spanned by P and u, v, w) are the loci of stationary (equilibrium) points on these sets of energy hypersurfaces, which are obtained by

$$\frac{\partial V}{\partial u} = \frac{\partial V}{\partial v} = \frac{\partial V}{\partial w} = 0 \tag{4}$$

Equations (4) represent a set of three nonlinear algebraic equations that must be satisfied for static equilibrium. One can now assume that one solution of these equilibrium equations, $u = u^F(P)$, $v = v^F(P)$, $w = w^F(P)$, defines a fundamental equilibrium path that is single valued at least in the domain of interest. The postbuckling equilibrium path (which is the physical continuation of the aforementioned fundamental path beyond the limit point) also is assumed to be single valued.

Recall that $V = U + \Omega$, where U is the positive definite function of the strain energy and Ω is the potential energy of the external load P. The expressions of these quantities are given by

$$U = \tfrac{1}{2}k_1\delta_1^2 + \tfrac{1}{2}k_2\delta_2^2 + \tfrac{1}{2}k_3\delta_3^2 + \tfrac{1}{2}k_4\delta_4^2$$
$$\Omega = -P(w - w_o) \tag{5}$$

where δ_i ($i = 1, 2, 3, 4$) are given in Eq. (3).

Subsequently, the dynamic response of the spring model when the point-load P is suddenly applied with infinite duration is examined, by taking into account the effects of geometric nonlinearities and damping. Assuming that the geometrically imperfect model under discussion is initially ($t = 0$) at rest, we can write for the preceding type of loading the following initial conditions:

$$u(0) = u_o, \qquad v(0) = v_o, \qquad w(0) = w_o$$
$$\dot{u}(0) = 0, \qquad \dot{v}(0) = 0, \qquad \dot{w}(0) = 0 \tag{6}$$

In view of conditions (6), the total energy E of the above autonomous model (including the loss of energy) at any time $t > 0$ is given by

$$E = V + K + 2\int_0^t F\,dt' = 0 \tag{7}$$

where V is a nonlinear function of the displacements (u, v, w) and linear function of the loading P; K is the positive definite function of the kinetic energy; and F is the positive definite dissipation function of Rayleigh. The analytical expressions of K and F are

$$K = \tfrac{1}{2}m(\dot{u}^2 + \dot{v}^2 + \dot{w}^2)$$
$$F = \tfrac{1}{2}c_1\dot{\delta}_1^2 + \tfrac{1}{2}c_2\dot{\delta}_2^2 + \tfrac{1}{2}c_3\dot{\delta}_3^2 + \tfrac{1}{2}c_4\dot{\delta}_4^2 \tag{8}$$

where c_i ($i = 1, 2, 3, 4$) are the coefficients of the viscous dampers of the four springs.

Usually, the integral in Eq. (7) is not integrable because of the form of its integrand; however, one could approximate this integral as follows:

$$\int_0^t \dot{\delta}_i^2\,dt' \geq \frac{1}{t}\left|\int_0^t \dot{\delta}_i\,dt'\right|^2 = \frac{1}{t}[\delta_i(t) - \delta_i(0)]^2 \tag{9}$$

where, from Eqs. (3), $\delta_i(0) = 0$ ($i = 1, 2, 3, 4$).

Then, from Eq. (7) it follows that

$$V + K \leq \left(-\frac{1}{t}\right)\sum_{i=1}^{4} c_i\delta_i^2 \tag{10}$$

where δ_i are given by Eqs. (3).

Lagrange equations of motion are given by

$$\frac{d}{dt}\left(\frac{\partial K}{\partial \dot{u}}\right) - \frac{\partial K}{\partial u} + \frac{\partial V}{\partial u} + \frac{\partial F}{\partial \dot{u}} = 0$$

$$\frac{d}{dt}\left(\frac{\partial K}{\partial \dot{v}}\right) - \frac{\partial K}{\partial v} + \frac{\partial V}{\partial v} + \frac{\partial F}{\partial \dot{v}} = 0 \tag{11}$$

$$\frac{d}{dt}\left(\frac{\partial K}{\partial \dot{w}}\right) - \frac{\partial K}{\partial w} + \frac{\partial V}{\partial w} + \frac{\partial F}{\partial \dot{w}} = 0$$

With the aid of relations (5), (8), and (3), Eqs. (11) become

$$m\ddot{u} - k_1(l_1' - l_{10})\frac{(l - u)}{l_1'} + k_2(l_2' - l_{20})\frac{(l + u)}{l_2'}$$
$$+ k_3(l_3' - l_{30})\frac{u}{l_3'} + k_4(l_4' - l_{40})\frac{u}{l_4'}$$
$$+ c_1\left[\frac{(l - u)\dot{u}}{l_1'} - \frac{v\dot{v}}{l_1'}\right]\frac{(l - u)}{l_1'} + c_2\left[\frac{(l + u)\dot{u}}{l_2'} + \frac{v\dot{v}}{l_2'}\right]$$
$$\times \frac{(l + u)}{l_2'} + c_3\left[-\frac{(h - w)\dot{w}}{l_3'} + \frac{(d + v)\dot{v}}{l_3'} + \frac{u\dot{u}}{l_3'}\right]\frac{u}{l_3'}$$
$$+ c_4\left[-\frac{(h - w)\dot{w}}{l_4'} - \frac{(d - v)\dot{v}}{l_4'} + \frac{u\dot{u}}{l_4'}\right]\frac{u}{l_4'} = 0$$

$$
\begin{aligned}
&m\ddot{v} + k_1(l_1' - l_{10})\frac{v}{l_1'} + k_2(l_2' - l_{20})\frac{v}{l_2'} \\
&+ k_3(l_3' - l_{30})\frac{(d+v)}{l_3'} - k_4(l_4' - l_{40})\frac{(d-v)}{l_4'} \\
&+ c_1\left[\frac{-(l-u)\dot{u}}{l_1'} + \frac{v\dot{v}}{l_1'}\right]\frac{v}{l_1'} + c_2\left[\frac{(l+u)\dot{u}}{l_2'} + \frac{v\dot{v}}{l_2'}\right]\frac{v}{l_2'} \\
&+ c_3\left[-\frac{(h-w)\dot{w}}{l_3'} + \frac{(d+v)\dot{v}}{l_3'} + \frac{u\dot{u}}{l_3'}\right]\frac{(d+v)}{l_3'} \\
&- c_4\left[-\frac{(h-w)\dot{w}}{l_4'} - \frac{(d-v)\dot{v}}{l_4'} + \frac{u\dot{u}}{l_4'}\right]\frac{(d-v)}{l_4'} = 0 \\
&m\ddot{w} - k_3(l_3' - l_{30})\frac{(h-w)}{l_3'} - k_4(l_4' - l_{40})\frac{(h-w)}{l_4'} \\
&- c_3\left[-\frac{(h-w)\dot{w}}{l_3'} + \frac{(d+v)\dot{v}}{l_3'} + \frac{u\dot{u}}{l_3'}\right]\frac{(h-w)}{l_3'} \\
&+ (-c_4)\left[-\frac{(h-w)\dot{w}}{l_4'} - \frac{(d-v)\dot{v}}{l_4'} + \frac{u\dot{u}}{l_4'}\right] \\
&\times \frac{(h-w)}{l_4'} - P = 0
\end{aligned}
\tag{12}
$$

where the expressions of l_i' and $l_{i0}\,(i = 1, 2, 3, 4)$ are given in Eqs. (1) and (2), respectively. Equations (12) along with the initial conditions (6) define a highly nonlinear initial-value problem. This, in general, can be solved only numerically, and hence a modified seventh-order numerical scheme of Runge–Kutta–Verner is employed herein. However, in the case of models with more than 3 DOF or in cases with some lack of reliability of large time solutions, one has to seek and consider all valuable information regarding the physical behavior of the model. Indeed, a thorough analysis of the dynamic buckling mechanism[5,7,8] allows us to apply qualitative criteria leading to readily obtained solutions of excellent accuracy for structural design purposes.

Because of the symmetry of the shell panel, it is reasonable to assume that

$$
\begin{aligned}
k_3 = k_4 = k, \qquad & \bar{k} = k_1/k = k_2/k \\
c_2 = c_1, \qquad & c_4 = c_3
\end{aligned}
\tag{13}
$$

Let us now introduce the following dimensionless quantities:

$$
\begin{aligned}
&q_1 = u/l, \qquad q_2 = v/l, \qquad q_3 = w/l, \qquad q_{10} = u_o/l \\
&q_{20} = v_o/l, \qquad q_{30} = w_o/l, \qquad \bar{d} = d/l \\
&\bar{h} = h/l(\bar{d}^2 + \bar{h}^2 = 1), \qquad \bar{l}_i = l_i'/l\,(i = 1, 2, 3, 4) \\
&\tau = t\sqrt{k/m}, \qquad \bar{c}_i = c_i/\sqrt{km} \quad (\text{with } \bar{c}_1 = \bar{c}_2 \text{ and } \bar{c}_3 = \bar{c}_4) \\
&\lambda = P/kl
\end{aligned}
\tag{14}
$$

Clearly, following from relations (12), we get

$$
\begin{aligned}
\bar{l}_1 &= \left[(1-q_1)^2 + q_2^2\right]^{\frac{1}{2}}, \qquad \bar{l}_2 = \left[(1+q_1)^2 + q_2^2\right]^{\frac{1}{2}} \\
\bar{l}_3 &= \left[(\bar{h}-q_3)^2 + (\bar{d}+q_2)^2 + q_1^2\right]^{\frac{1}{2}} \\
\bar{l}_4 &= \left[(\bar{h}-q_3)^2 + (\bar{d}-q_2)^2 + q_1^2\right]^{\frac{1}{2}}
\end{aligned}
\tag{15}
$$

Equations (12), by virtue of relations (13–15), become

$$
\begin{aligned}
&\ddot{q}_1 - \bar{k}\left(1 - \frac{\beta_1}{\bar{l}_1}\right)(1-q_1) + \bar{k}\left(1 - \frac{\beta_2}{\bar{l}_2}\right)(1+q_1) \\
&+ \left(1 - \frac{\beta_3}{\bar{l}_3}\right)\bar{q}_1 + \left(1 - \frac{\beta_4}{\bar{l}_4}\right)q_1 \\
&+ \left\{\bar{c}_1\left[\frac{(1-q_1)^2}{\bar{l}_1^2} + \frac{(1+q_1)^2}{\bar{l}_2^2}\right] + \bar{c}_3\left(\frac{1}{\bar{l}_3^2} + \frac{1}{\bar{l}_4^2}\right)q_1^2\right\}\dot{q}_1 \\
&+ \left\{-\bar{c}_1\left[\frac{1-q_1}{\bar{l}_1^2} - \frac{1+q_1}{\bar{l}_2^2}\right]q_2\right. \\
&\left.+ \bar{c}_3\left[\frac{(\bar{d}+q_2)}{\bar{l}_3^2} - \frac{(\bar{d}-q_2)}{\bar{l}_4^2}\right]q_1\right\}\dot{q}_2 \\
&- \bar{c}_3\left(\frac{1}{\bar{l}_3^2} + \frac{1}{\bar{l}_4^2}\right)(\bar{h}-q_3)q_1\dot{q}_3 = 0
\end{aligned}
\tag{16a}
$$

$$
\begin{aligned}
&\ddot{q}_2 + \bar{k}\left(2 - \frac{\beta_1}{\bar{l}_1} - \frac{\beta_2}{\bar{l}_2}\right)q_2 + \left(1 - \frac{\beta_3}{\bar{l}_3}\right)(\bar{d}+q_2) \\
&- \left(1 - \frac{\beta_4}{\bar{l}_4}\right)(\bar{d}-q_2) + \left\{\bar{c}_1\left[-\frac{(1-q_1)}{\bar{l}_1^2} + \frac{(1+q_1)}{\bar{l}_2^2}\right]q_2\right. \\
&\left.+ \bar{c}_3\left[\frac{(\bar{d}+q_2)}{\bar{l}_3^2} - \frac{(\bar{d}-q_2)}{\bar{l}_4^2}\right]q_1\right\}\dot{q}_1 \\
&+ \left\{\left[\bar{c}_1\left(\frac{1}{\bar{l}_1^2} + \frac{1}{\bar{l}_2^2}\right)q_2^2\right] + \bar{c}_3\left[\frac{(\bar{d}+q_2)^2}{\bar{l}_3^2} + \frac{(\bar{d}-q_2)^2}{\bar{l}_4^2}\right]\dot{q}_2\right\} \\
&+ \bar{c}_3\left[-\frac{(\bar{d}+q_2)}{\bar{l}_3^2} + \frac{(\bar{d}-q_2)}{\bar{l}_4^2}\right](\bar{h}-q_3)\dot{q}_3 = 0
\end{aligned}
\tag{16b}
$$

$$
\begin{aligned}
&\ddot{q}_3 - \left(2 - \frac{\beta_3}{\bar{l}_3} - \frac{\beta_4}{\bar{l}_4}\right)(\bar{h}-q_3) - \bar{c}_3\left(\frac{1}{\bar{l}_3^2} + \frac{1}{\bar{l}_4^2}\right)(\bar{h}-q_3)q_1\dot{q}_1 \\
&+ \bar{c}_3\left[-\frac{(\bar{d}+q_2)}{\bar{l}_3^2} + \frac{(\bar{d}-q_2)}{\bar{l}_4^2}\right](\bar{h}-q_3)\dot{q}_2 \\
&+ \bar{c}_3\left(\frac{1}{\bar{l}_3^2} + \frac{1}{\bar{l}_4^2}\right)(\bar{h}-q_3)^2\dot{q}_3 - \lambda = 0
\end{aligned}
\tag{16c}
$$

where

$$
\begin{aligned}
\beta_1 &= \left[q_{20}^2 + (1-q_{10})^2\right]^{\frac{1}{2}}, \qquad \beta_2 = \left[q_{20}^2 + (1+q_{10})^2\right]^{\frac{1}{2}} \\
\beta_3 &= \left[(\bar{h}-q_{30})^2 + (\bar{d}+q_{20})^2 + q_{10}^2\right]^{\frac{1}{2}} \\
\beta_4 &= \left[(\bar{h}-q_{30})^2 + (\bar{d}-q_{20})^2 + q_{10}^2\right]^{\frac{1}{2}}
\end{aligned}
\tag{17}
$$

The initial conditions (6) using Eqs. (14) become

$$
\begin{aligned}
&q_1(0) = q_{10}, \qquad q_2(0) = q_{20}, \qquad q_3(0) = q_{30} \\
&\dot{q}_1(0) = 0, \qquad \dot{q}_2(0) = 0, \qquad \dot{q}_3(0) = 0
\end{aligned}
\tag{18}
$$

Setting $\ddot{q}_i = \dot{q}_i = 0\,(i = 1, 2, 3)$ (neglecting inertia terms) in Eqs. (16), we obtain the following nonlinear equilibrium equations:

$$
\begin{aligned}
&-\bar{k}\left(1 - \frac{\beta_1}{\bar{l}_1}\right)(1-q_1) + \bar{k}\left(1 - \frac{\beta_2}{\bar{l}_2}\right)(1+q_1) + \left(2 - \frac{\beta_3}{\bar{l}_3} - \frac{\beta_4}{\bar{l}_4}\right)q_1 = 0 \\
&\bar{k}\left(2 - \frac{\beta_1}{\bar{l}_1} - \frac{\beta_2}{\bar{l}_2}\right)q_2 + \left(1 - \frac{\beta_3}{\bar{l}_3}\right)(\bar{d}+q_2) - \left(1 - \frac{\beta_4}{\bar{l}_4}\right)(\bar{d}-q_2) = 0 \\
&\left(2 - \frac{\beta_3}{\bar{l}_3} - \frac{\beta_4}{\bar{l}_4}\right)(\bar{h}-q_3) + \lambda = 0
\end{aligned}
\tag{19}
$$

It follows from relation (14) that the total energy equation (7), in dimensionless form, is equal to

$$E = E/kl^2 = V + K + 2\int_0^\tau F\,d\tau' = 0 \tag{20}$$

where

$$\begin{aligned} V = V/kl^2 &= \tfrac{1}{2}\bar{k}\left\{\left[q_2^2 + (1-q_1)^2\right]^{\frac{1}{2}} - \beta_1\right\}^2 \\ &+ \tfrac{1}{2}\bar{k}\left\{\left[q_2^2 + (1+q_1)^2\right]^{\frac{1}{2}} - \beta_2\right\}^2 \\ &+ \tfrac{1}{2}\left\{\left[(\bar{h}-q_3)^2 + (\bar{d}+q_2)^2 + q_1^2\right]^{\frac{1}{2}} - \beta_3\right\}^2 \\ &+ \tfrac{1}{2}\left\{\left[(\bar{h}-q_3)^2 + (\bar{d}-q_2)^2 + q_1^2\right]^{\frac{1}{2}} - \beta_4\right\}^2 - \lambda(q_3 - q_{30}) \end{aligned}$$

$$K = \tfrac{1}{2}\left(\dot{q}_1^2 + \dot{q}_2^2 + \dot{q}_3^2\right) \tag{21}$$

$$\begin{aligned} 2F &= \bar{c}_1\left\{\frac{[q_2\dot{q}_2 - (1-q_1)\dot{q}_1]^2}{\bar{l}_1^2} + \frac{[q_2\dot{q}_2 + (1+q_1)\dot{q}_1]^2}{\bar{l}_2^2}\right\} \\ &+ \bar{c}_3\left\{\frac{[(\bar{h}-q_3)\dot{q}_3 - (\bar{d}+q_2)\dot{q}_2 + q_1\dot{q}_1]^2}{\bar{l}_3^2}\right. \\ &\left. + \frac{[(\bar{h}-q_3)\dot{q}_3 - (\bar{d}-q_2)^2\dot{q}_2 + q_1\dot{q}_1]^2}{\bar{l}_4^2}\right\} \end{aligned}$$

Equation (10), in dimensionless form, becomes

$$V + K \le \left\{-(1/\tau)\left[\bar{c}_1\left(\bar{\delta}_1^2 + \bar{\delta}_2^2\right) + \bar{c}_3\left(\bar{\delta}_3^2 + \bar{\delta}_4^2\right)\right]\right\} \tag{22}$$

where the expression of time τ (until dynamic buckling) is unknown and $\bar{\delta}_i\,(i = 1, 2, 3, 4)$ are given by

$$\begin{aligned} \bar{\delta}_1 &= \delta_1/l = \left[q_2 + (1-q_1)^2\right]^{\frac{1}{2}} - \left[q_{20} + (1-q_{10})^2\right]^{\frac{1}{2}} \\ \bar{\delta}_2 &= \delta_2/l = \left[q_2 + (1+q_1)^2\right]^{\frac{1}{2}} - \left[q_{20} + (1+q_{10})^2\right]^{\frac{1}{2}} \\ \bar{\delta}_3 &= \delta_3/l = \left[(\bar{h}-q_3)^2 + (\bar{d}+q_2)^2 + q_1^2\right]^{\frac{1}{2}} \\ &- \left[(\bar{h}-q_{30})^2 + (\bar{d}+q_{20})^2 + q_{10}^2\right]^{\frac{1}{2}} \\ \bar{\delta}_4 &= \delta_4/l = \left[(\bar{h}-q_3)^2 + (\bar{d}-q_2)^2 + q_1^2\right]^{\frac{1}{2}} \\ &- \left[(\bar{h}-q_{30})^2 + (\bar{d}-q_{20})^2 + q_{10}^2\right]^{\frac{1}{2}} \end{aligned} \tag{23}$$

Although an exact evaluation of the time τ is impossible, however, due to the fact that the numerator of the right-hand side of Eq. (22) is a very small quantity, approximate values of τ give very good results. Thus from condition (7) or (20), it is clear that throughout the motion, including dynamic buckling (escaped motion) the total potential energy satisfies the inequality

$$V \le 0 \tag{24}$$

Hence, there is no motion (and dynamic buckling as well) if $V > 0$. Moreover, when the motion passes through an unstable equilibrium position (saddle point), the total kinetic energy is zero, $K = 0$, whereas according to condition (24), it is negative (if damping is not zero) or zero (for zero damping). Furthermore, if the motion passes through the stable equilibrium position, K becomes maximum and V becomes minimum.

In the case of a nondissipative model, but with vanishing nonzero damping (i.e., when $c_i \to 0$ for $i = 1, 2, 3, 4$), then

$$K + V = 0 \tag{25}$$

According to previous analyses,[7,8] dynamic buckling occurs via a saddle (or its neighborhood), satisfying condition (24). Then, a lower-bound dynamic buckling load $\tilde{\lambda}_D$ is obtained by solving the equilibrium equations (19) together with condition (24) with respect to $q_i\,(i = 1, 2, 3)$ and λ. Moreover, if λ_D corresponds to the nondissipative model (i.e., $c_i = 0$ for $i = 1, 2, 3, 4$), then $\tilde{\lambda}_D < \lambda_D$, whereas for a dissipative model the following inequalities are valid[5,9]:

$$\tilde{\lambda}_D < \lambda_D < \lambda_{DD} < \lambda_s < \lambda_c \tag{26}$$

where λ_s is the (static) limit point load, and λ_c is the bifurcational load of the perfect model from which the imperfect (limit point) system is generated.

If

$$\bar{q} = q_1 i + q_2 j + q_3 k \qquad \left(q = \sqrt{q_1^2 + q_2^2 + q_3^2}\right) \tag{27}$$

then, for a nondissipative model, condition (25), by virtue of Eq. 19, yields

$$\dot{q}^2 = -2V \qquad \text{or} \qquad d\tau = \frac{dq}{\sqrt{-2V}} \tag{28}$$

Note that V (being a very small negative quantity throughout the motion) varies little. At $\tau = 0$, $V = 0$; at the stable equilibrium position, q^E becomes minimum [i.e., $V^E = \min$, which is readily determined from Eq. (21) for $\lambda = \tilde{\lambda}_D$ and $q_i = q_i^E$]; and at the saddle point $(\tilde{\lambda}_D, q_i^D)$ again, $V = 0$. On the basis of these three values of V, one can adopt an average value

$$\tilde{\tau}_D \cong \frac{1}{\sqrt{-2V_{\text{av}}}}\left[\left(q_1^D - q_{10}\right)^2 + \left(q_2^D - q_{20}\right)^2 + \left(q_3^D - q_{30}\right)^2\right]^{\frac{1}{2}} \tag{29}$$

where $\tilde{\tau}_D$ is an approximate value of the time up to dynamic buckling for a nondissipative model.

In case of a dissipative model, one can solve the equilibrium equations (19) together with condition (22), where τ is taken approximately equal to $\tilde{\tau}_D$ given by Eq. (29). However, a better estimate for τ_D could be obtained if, in formula (29), the quantity under the radical were replaced by

$$-2V_{\text{av}} - (2/\tilde{\tau}_D)\left[\bar{c}_1\left(\bar{\delta}_1^2 + \bar{\delta}_2^2\right) + \bar{c}_3\left(\bar{\delta}_3^2 + \bar{\delta}_4^2\right)\right] \tag{30}$$

where $\bar{\delta}_i$ are given in Eq. (23), with $q_i = q_i^D\,(i = 1, 2, 3)$ obtained from the system of Eqs. (19) and (24). Because dynamic buckling is usually accompanied by nonlinear oscillations about either the asymptotically stable equilibrium state or (rarely) about the saddle (or its neighborhood), it is clear that the time $\tilde{\tau}_D$ or τ_D is a lower bound of the exact time (until dynamic buckling).

III. New Dynamic Buckling Estimates

On the basis of several observations regarding the surface or hypersurface of $V \le 0$ in the V-q space on which the motion is taking place and its implication on the difference between $\tilde{\lambda}_D$ (associated with $V = 0$) and λ_D corresponding to the nondissipative model, one can predict the conditions under which $\tilde{\lambda}_D$ approaches λ_D. Subsequently, with the aid of $\tilde{\lambda}_D$ one can establish an approximate load $\bar{\lambda}_{DD}$ very close to the exact dynamic buckling load λ_{DD} of the corresponding dissipative model.

For simplicity, one can first consider a 2-DOF model and then extend the analysis to a multi-DOF model.

With the aid of Fig. 3a, one can see the nonlinear equilibrium path AESDG. The stable equilibrium point $E\,(q_1^E, q_2^E)$ and the unstable $D\,(q_1^D, q_2^D)$ correspond to the same load $\tilde{\lambda}_D$ obtained via the solution of Eqs. (19) and condition $V = 0$. The total potential energy surface in the V-q_i space for the fixed value $\lambda = \tilde{\lambda}_D$ is depicted in Fig. 3b. The motion starts from point $A\,(q_{10}, q_{20})$ with $V = 0$; thereafter, it is taking place on the V surface with $V \le 0$ (namely, below the horizontal plane $q_1 0 q_2$) with an overall direction to approach the saddle point D with $\partial V/\partial q_1 = \partial V/\partial q_2 = 0$. Point D corresponds to a local maximum in a certain direction within the surface $V < 0$ and to a local minimum in the normal to the previous direction. In 1-DOF models, there is only one trajectory from the starting point A to the saddle point D through which (or its neighborhood) an escaped motion (dynamic buckling) occurs. However, for 2-DOF models, an escaped motion is possible if the starting motion (trajectory) from point A follows a path on the V surface that passes through the saddle D in the direction of its maximum.

If this happens (which, in general, is improbable), then $\tilde{\lambda}_D \equiv \lambda_D$. However, because of the existence of many trajectories starting point A, the motion cannot follow the unique previous path leading to the

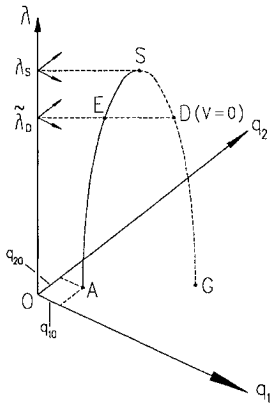

Fig. 3a Limit point model.

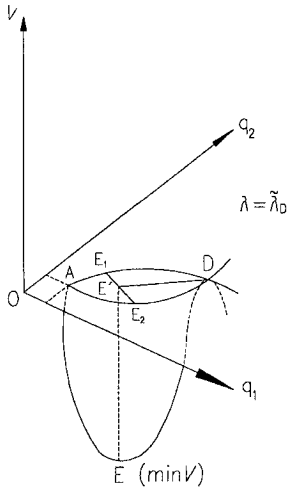

Fig. 3b Total potential energy surface corresponding to $\tilde{\lambda}_D$.

saddle point D, and thus, before approaching point D, it returns following a different path on the $V(\leq 0)$ surface. Then, a new motion starts with an overall tendency to be directed to the saddle point D, and because this is usually unlikely, the motion comes back again. In this way, we have nonlinear oscillations around the stable equilibrium state q^E whose amplitudes do not approach the saddle point D, and thus dynamic buckling (escaped motion) is impossible, because there is no trajectory passing via the saddle D in the direction of its maximum. However, if the channel within which the motion takes place (which is defined by the space between the horizontal plane and the surface $V < 0$ in the V-q_i space) is slender enough, then $\tilde{\lambda}_D$ approaches λ_D. More specifically, the more slender the motion channel is, the less the difference between $\tilde{\lambda}_D$ and λ_D becomes. The slenderness of the motion channel depends on the length ratio AD (distance between the stable and the unstable points) vs E_1E_2 (see Fig. 3b), where E_1E_2 is the distance between the two boundaries with $V = 0$ (which are the intersections of the V surface with the horizontal plane). As this ratio increases, the difference between $\tilde{\lambda}_D$ and λ_D decreases, because in this case the channel of motion prior to the saddle point D becomes slenderer and narrower, having an overall tendency to be identified by one trajectory. Certainly, the slenderness of the motion channel depends also on the min V, which corresponds to the stable equilibrium point (q_1^E, q_2^E).

Moreover, the difference between λ_D and $\tilde{\lambda}_D$ depends also on the possible existence of local oscillations of the model (in addition to the global ones) and (mainly) on the model DOF as well. The latter is very important, because as the DOF increases, additional constraints to the motion are introduced. Establishment of the relationship between the difference $(\lambda_D - \tilde{\lambda}_D)$ and the aforementioned parameters is an interesting but difficult task.

Instead of this, an approximate (rather, upper-bound) dynamic buckling load $\bar{\lambda}_D$ for a nondissipative model is proposed that is higher than $\tilde{\lambda}_D$ and closer to the exact load λ_D. The reasoning for the derivation of $\bar{\lambda}_D$ is based on the mere observation that the probability of any motion starting from point A to find the escape passage leading to dynamic buckling increases with the enlargement of the escape passage. This is achieved if the saddle point D is going down (see Fig. 3b) in the V-q_i space, which is accomplished by increasing the load λ above $\tilde{\lambda}_D$. Clearly, the possibility for dynamic buckling (escaped motion) increases considerably if the point D descends down to the level of point E (associated with $V^E = \min V$). Then, the approximate dynamic buckling load $\bar{\lambda}_D$ and the corresponding displacements $\bar{q}_1^D$ and $\bar{q}_2^D$ are obtained by solving the system of equilibrium equations (19), together with the condition

$$V = V^E \tag{31}$$

We must always have in mind that solution sought corresponds to a saddle on the unstable postbuckling path.

It is not difficult to extend the preceding development to the case of models with more than 2 DOF. For the 3-DOF nondissipative model under discussion, the approximate dynamic buckling load $\bar{\lambda}_D$ (and the respective displacements $\bar{q}_1^D$, $\bar{q}_2^D$, and $\bar{q}_3^D$) are easily determined by solving the system of algebraic equations (19) together with condition (31), where V^E corresponds to the stable equilibrium point (q_1^E, q_2^E, q_3^E) associated with $V = 0$. However, as stated above for a 3-DOF model, $\tilde{\lambda}_D$ is very close to λ_D, and then $\bar{\lambda}_D$ can be considered as an upper bound.

For a dissipative model with given damping coefficients $c_i (c_1 = c_2, c_3 = c_4)$, the condition $V = 0$ is replaced by [see Eq. (22)]

$$V = -(1/\tilde{\tau}_D)\left[\bar{c}_1\left(\bar{\delta}_1^2 + \bar{\delta}_2^2\right) + \bar{c}_3\left(\bar{\delta}_3^2 + \bar{\delta}_4^2\right)\right] \tag{32}$$

where $\bar{\delta}_i$ are given in Eqs. (23), $q_i = \bar{q}_i^D$ (of the nondissipative model), and $\tilde{\tau}_D$ is obtained either from Eq. (29) by replacing q_i^D by $\bar{q}_i^D$ or from Eqs. (29) and (30).

IV. Discussion of Numerical Results

Numerical results of the nonlinear static stability analysis are presented first as a necessary prerequisite to understanding the dynamic buckling phenomenon. All findings are in graphic and tabular forms, and thereafter checked via a modified seventh-order scheme of Runge–Kutta–Verner.

A. Nonlinear Static Buckling

The system of nonlinear equilibrium equations (19) can be solved readily with respect to q_i $(i = 1, 2, 3)$ by step-increasing the loading λ for various values of the stiffness ratio $\bar{k}(1, 0.5)$ and of the length ratio $\bar{d}(0.5)$ for given initial conditions $(q_{i0} = 0.01$ for $i = 1, 2, 3)$. Nonlinear equilibrium paths can be established graphically as plots of the loading λ against any characteristic displacement $q_i (i = 1, 2, 3)$ or against $q = (q_1^2 + q_2^2 + q_3^2)^{1/2}$. The fact that stiffness is provided mainly by springs 3 and 4 and secondarily by springs 1 and 2 is reflected by the typical plots λ vs q_1 and λ vs q_3 (see Figs. 4a and 4b), where the corresponding equilibrium paths increase continuously up to the limit point S, as λ increases. However, this is not the case for the plot λ vs q_2 (Fig. 4c). The dashed lines in these plots represent unstable equilibrium paths whose equilibrium (saddle) points are associated with second variations of the total potential energy V, which are indefinite.

In Fig. 5, one can see the typical plot of a nonlinear equilibrium path λ vs $q = (q_1^2 + q_2^2 + q_3^2)^{1/2}$. Note also that, in addition to the above physical (primary and secondary) paths, there are complementary (physically unacceptable) equilibrium paths, which are not depicted in Figs. 4a–4c and 5. All of the plots in Fig. 5 correspond to $\bar{k} = 1$. If $\bar{k} = 0.50$ (while all other parameters remain constant), the forms of all of the equilibrium paths in Fig. 5 change very little, except that of λ vs q_2, as shown in Fig. 6.

It is important for the subsequent dynamic buckling analysis check whether all stable equilibria (represented by continuous lines) can act as point attractors.

B. Nonlinear Dynamic Buckling

In all of the nonlinear equilibrium paths in Fig. 6, one can see the saddle point D (on the unstable postbuckling path), which is associated with zero total potential energy, $V = 0$. This condition, along with the equilibrium equations (19), yields the (lower-bound) dynamic estimate $\tilde{\lambda}_D$ associated with a nondissipative model (i.e., $\tilde{\lambda}_D < \lambda_D$). As mentioned above, the accuracy of $\tilde{\lambda}_D$ depends on the slenderness ratio of the motion channel and more specifically on the

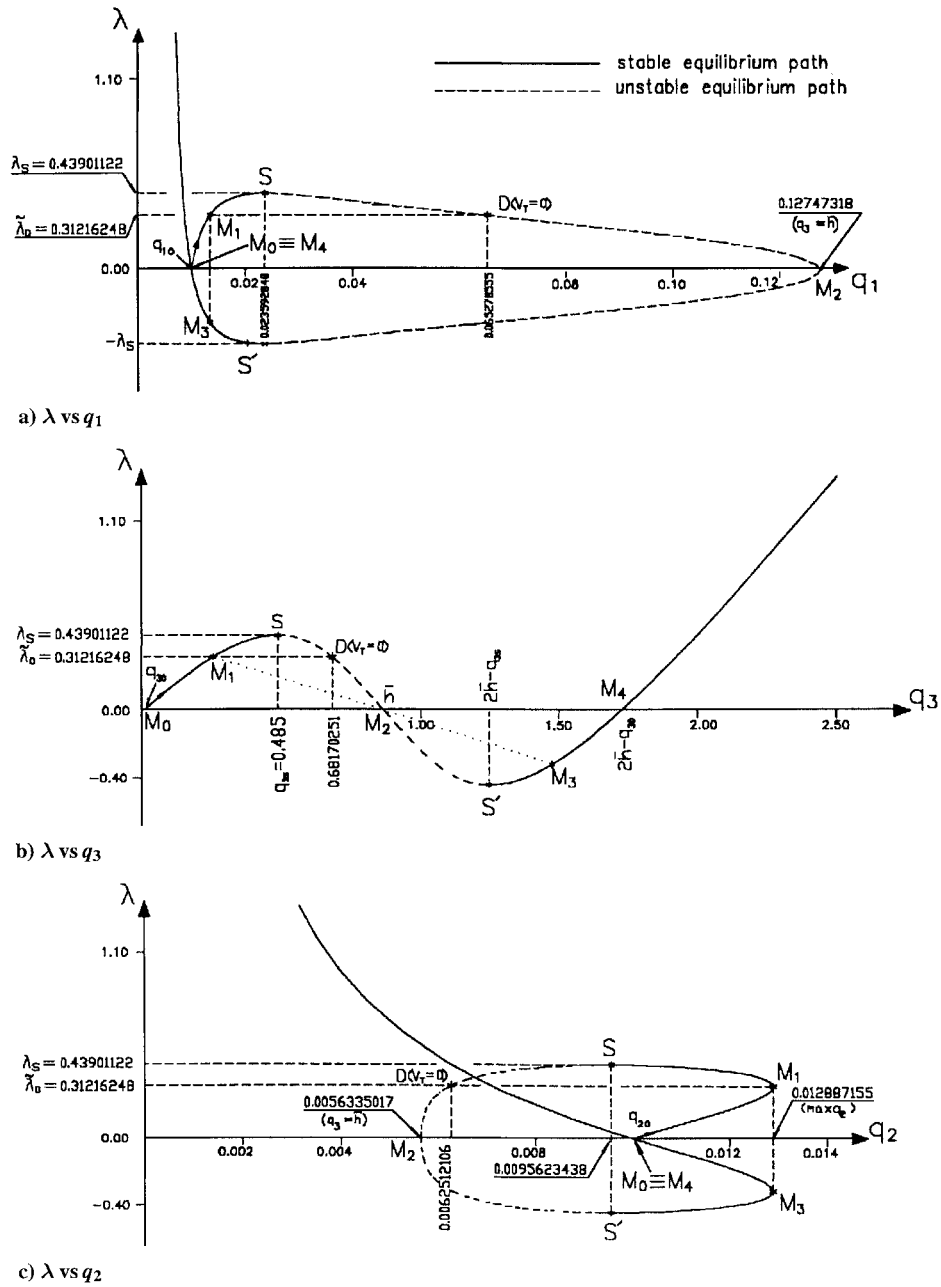

Fig. 4 Physical equilibrium paths (λ vs q_i) for a model with $\bar{k} = 1, \bar{d} = 0.50$ ($\bar{d}^2 + \bar{h}^2 = 1$), and $q_{i0} = 0.01$ ($i = 1, 2, 3$).

length ratio $(DE)/(E_1E_2)$, where both distances (DE) and (E_1E_2) are taken in plane normal to the V axis (see Fig. 3b). Because stiffness, as was stated, is mainly provided by q_1 and q_3, one can consider basically the (horizontal) plane $0q_1q_3$ (normal to the V axis). The other (horizontal) planes clearly restrict further the motion channel, which thus becomes narrower. This implies a decrease in the difference $\lambda_D - \tilde{\lambda}_D$. In Fig. 7, one can see the boundary $V = 0$ between motion and no motion, the saddle point D, the projection E' of the equilibrium point E on the horizontal plane, the distances (DE) and (E_1E_2) for the case of a nondissipative model with $\bar{k} = 1, \bar{d} = 0.50$, $q_{10} = q_{20} = q_{30} = 0.01$. The aforementioned length ratio $(DE)/(E_1E_2)$ is appreciably affected by the stiffness ratio $\bar{k}$ (i.e., the stiffness of springs 1 and 2 vs the stiffness of springs 3 and 4).

Table 1, corresponding to a model with $\bar{d} = 0.50, q_{10} = q_{20} = q_{30} = 0.01$, gives for varying values of $\bar{k}(1, 0.5)$ a number of numerical results: the length ratio $(DE)/(E_1E_2)$, the saddle displacements $\tilde{q}_i^D (i = 1, 2, 3)$, the displacements $q_i^E (i = 1, 2, 3)$ of the stable equilibrium path, the load $\tilde{\lambda}_D$, the load λ_D (obtained via Runge–Kutta–Verner), the potential $V^E = V(q_i^E; \tilde{\lambda}_D)$ and the approximate dynamic buckling load $\bar{\lambda}_D$ based on V^E [see Eq. (31)]. From these results, it is clear that as the ratio $(DE)/(E_1E_2)$ increases and $(E_1E_2) \gg |V^E|$, the difference $\lambda_D - \tilde{\lambda}_D$ decreases. Moreover, the approximate load $\bar{\lambda}_D$ is an upper bound of λ_D better than λ_s. For systems with more than 3 DOF, additional restraints are introduced, rendering the motion channel narrower, which implies reduction in the difference $\lambda_D - \tilde{\lambda}_D$, this also happens when more DOF are introduced, because the motion channel becomes slenderer. The starting point of motion (in the motion channel) in connection with the points of the saddle and the corresponding stable equilibrium point plays a very important role. More details about the accuracy of the proposed dynamic buckling loads are given by Gantes and Kounadis.[10]

C. Dissipative Model

Using the approximate relations (22), (29), and/or (30), one can evaluate, for instance, the approximate dynamic buckling load $\bar{\lambda}_{DD}$ for the case $\bar{c}_1 = \bar{c}_2 = 0.02, \bar{c}_3 = \bar{c}_4 = 0.05$, corresponding to the cases $\bar{k} = 0.50$ and 1.00 (Table 1). Then we find $\bar{k} = 0.50 : \bar{\lambda}_{DD} =$

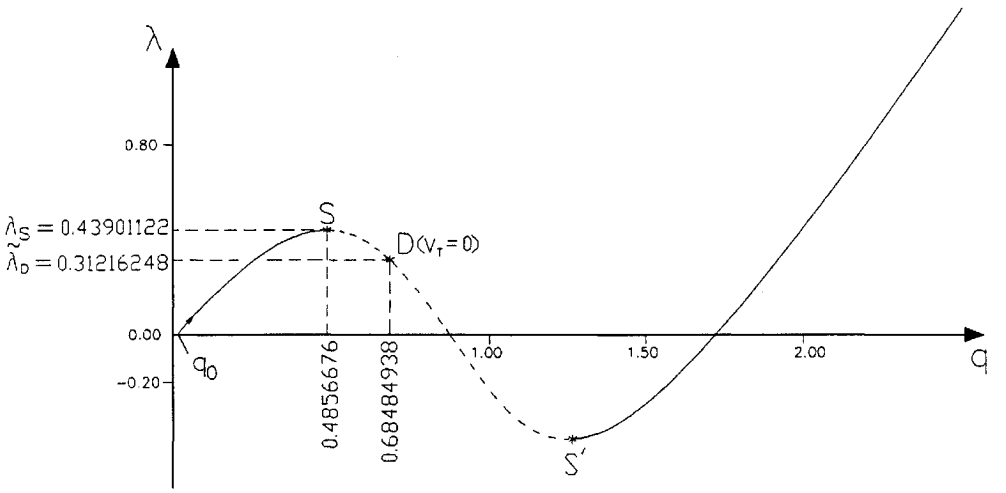

Fig. 5 Physical equilibrium path (λ vs q_i) [$q = (q_1^2 + q_2^2 + q_3^2)^{1/2}$] for a model with $\bar{k} = 1, \bar{d} = 0.50$, and $q_{i0} = 0.01$ ($i = 1, 2, 3$).

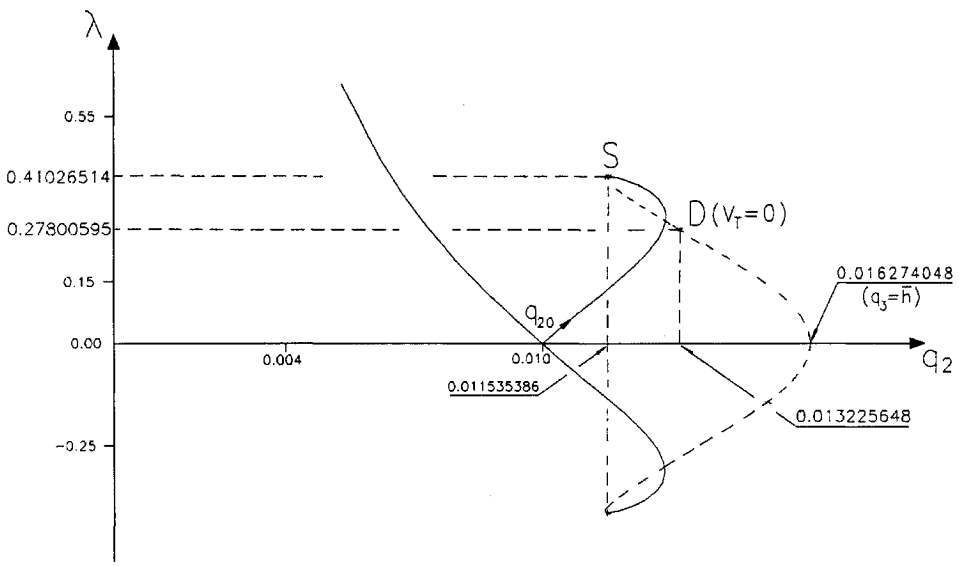

Fig. 6 Physical equilibrium path (λ vs q_i) for a model with $\bar{k} = 0.50, \bar{d} = 0.50$ ($\bar{d}^2 + \bar{h}^2 = 1$), and $q_{i0} = 0.01$ ($i = 1, 2, 3$).

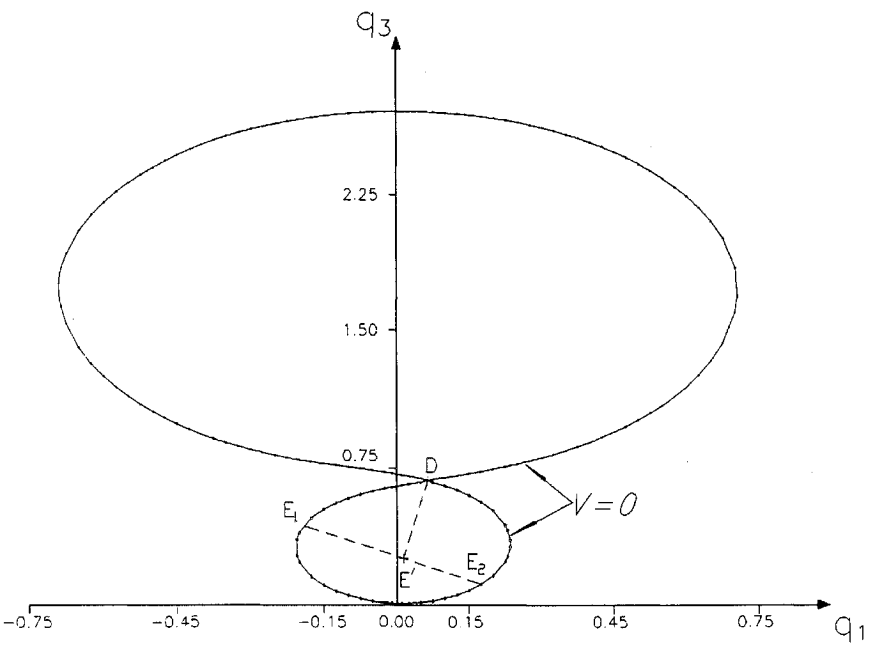

Fig. 7 Boundary between motion and no motion and projection of motion channel dimensions on plane $0q_1q_3$ for a model with $\bar{k} = 1.00, \bar{d} = 0.50$, and $q_{i0} = 0.01$ ($i = 1, 2, 3$).

Table 1 Exact and approximate dynamic buckling loads and corresponding motion channel geometry for a nondissipative model with $\bar{d} = 0.50$, $q_{i0} = 0.01$ $(i = 1, 2, 3)$, and various values of $\bar{k}$

		Saddle point ($V_T = 0$)			Corresponding stable equilibrium position						
$\bar{k}$	DE/E_1E_2[a]	$\tilde{q}_1^D$	$\tilde{q}_2^D$	$\tilde{q}_3^D$	q_1^E	q_2^E	q_3^E	$\tilde{\lambda}_D$[b]	λ_D[c]	V^E[d]	$\bar{\lambda}_D, V^E = V_T$
0.5[e]	0.8027	0.33709	0.01323	0.57946	0.0176	0.01282	0.22219	0.27801	0.2881	−0.02798	0.32962
0.6	0.8172	0.28312	0.01081	0.6125	0.01636	0.01287	0.23664	0.29344	0.31012	−0.03136	0.34769
0.7	0.8172	0.22698	0.00889	0.63941	0.01537	0.01289	0.24617	0.30326	0.31095	−0.03363	0.35863
0.8	0.857	0.16751	0.0075	0.66075	0.01458	0.01289	0.25158	0.30881	0.31193	−0.03495	0.36428
0.9	0.9191	0.10772	0.00662	0.67537	0.01394	0.01288	0.25406	0.31131	0.31237	−0.03555	0.36653
1[f]	0.979	0.06528	0.00625	0.6817	0.01343	0.01288	0.25489	0.31216	0.31254	−0.03576	0.36725
1.25	1.1408	0.03208	0.00609	0.68435	0.01257	0.01288	0.25533	0.31263	0.31271	−0.03587	0.36771
1.5	1.2719	0.02352	0.00607	0.68469	0.01206	0.01288	0.25543	0.31274	0.31278	−0.03589	0.36783
1.75	1.391	0.01973	0.00607	0.68481	0.01172	0.01288	0.25547	0.31278	0.31279	−0.03591	0.36788
2	1.5014	0.0176	0.00606	0.68487	0.01147	0.01288	0.2555	0.31281	0.31284	−0.03592	0.36792
3	1.8796	0.01404	0.00606	0.68493	0.01093	0.01288	0.25552	0.31286	0.31291	−0.03593	0.36797
4	2.1942	0.01275	0.00606	0.68495	0.01068	0.01288	0.25553	0.31288	0.31293	−0.03593	0.36799
5	2.4692	0.01209	0.00605	0.68496	0.01054	0.01287	0.25554	0.31288	0.31291	−0.03593	0.368

[a]Channel length/channel width. [b]$V_T = 0$. [c]Runge–Kutta–Verner scheme. [d]Channel depth. [e]$\lambda_s = 0.41326514$. [f]$\lambda_s = 0.43901122$.

0.29985099, $\bar{k} = 1.00 : \bar{\lambda}_{DD} = 0.3146453$, whereas the exact ones are 0.31917336 and 0.3224387, respectively.

V. Conclusions

The most important conclusions based on a one-mass 3-DOF model are the following:

1) The dynamic buckling response of the preceding imperfect dissipative model simulating a relatively deep cylindrical shell panel under a step loading is comprehensively presented using the modern theory of nonlinear dynamics.

2) Energy, topological, and geometric criteria allow us to readily establish dynamic buckling loads of very good accuracy for structural design purposes, without integrating the highly nonlinear initial-value problem.

3) An a priori knowledge of the accuracy of the above dynamic buckling loads is obtained by discussing the geometry of the motion channel and the starting point of motion (within this channel), in connection with the location of the saddle and corresponding to the same load $\bar{\lambda}_D$ stable equilibrium point.

References

[1]Simitses, G. J., *Dynamic Stability of Suddenly Loaded Structures*, Springer–Verlag, New York, 1990.

[2]Greer, J. M., and Palazotto, A. N., "Nonlinear Dynamics of a Simple Shell Model with Chaotic Snapping Behavior," *Journal of Engineering Mechanics*, Vol. 121, No. 6, 1995, pp. 753–761.

[3]Budiansky, B., "Dynamic Buckling of Elastic Structures: Criteria and Estimates," *Dynamic Stability of Structures*, edited by G. Hermann, Pergamon, Oxford, England, UK, 1967, pp. 83–106.

[4]Elishakoff, I., "Remarks on the Static and Dynamic Imperfection-Sensitivity of Nonsymmetric Structures," *Journal of Applied Mechanics*, Vol. 47, 1980, pp. 111–115.

[5]Kounadis, A. N., "A Qualitative Analysis for the Local and Global Dynamic Buckling and Stability of Autonomous Discrete Systems," *Quarterly Journal of Mechanics and Applied Mathematics*, Vol. 47, No. 2, 1994, pp. 269–295.

[6]Chien, L. S., and Palazotto, A. N., "Dynamic Buckling of Composite Cylindrical Panels with High-Order Transverse Shears Subjected to a Transverse Concentrated Load," *International Journal of Non-Linear Mechanics*, Vol. 27, No. 5, 1992, pp. 719–734.

[7]Kounadis, A. N., "Qualitative Criteria in Nonlinear Dynamic Buckling and Stability of Autonomous Dissipative Systems," *International Journal of Non-Linear Mechanics* (to be published).

[8]Kounadis, A. N., "On the Dynamic Buckling Mechanism of Autonomous Dissipative/Nondissipative Structural Systems," *Archives of Mechanics* (to be published).

[9]Kounadis, A. N., "Static and Dynamic, Local and Global, Bifurcations in Nonlinear Autonomous Structural Systems," *AIAA Journal*, Vol. 31, No. 8, 1993, pp. 1468–1477.

[10]Gantes, C. J., and Kounadis, A. N., "Qualitative Criteria for Establishing Dynamic Buckling Loads of Autonomous Dissipative Systems," 19th International Congress of Theoretical and Applied Mechanics, Kyoto, Japan, 1996.